A two-step automated procedure based on adaptive limit and pushover analyses for the seismic assessment of masonry structures

Published Version:
D'Altri A.M., Lo Presti N., Grillanda N., Castellazzi G., de Miranda S., Milani G. (2021). A two-step automated procedure based on adaptive limit and pushover analyses for the seismic assessment of masonry structures. COMPUTERS & STRUCTURES, 252, 1-15 [10.1016/j.compstruc.2021.106561].

Availability:
This version is available at: https://hdl.handle.net/11585/841967 since: 2021-12-16

Published:
DOI: http://doi.org/10.1016/j.compstruc.2021.106561

A two-step automated procedure based on adaptive limit and pushover analyses for the seismic assessment of masonry structures

Antonio Maria D'Altri[1], Nicolò Lo Presti[1], Nicola Grillanda[2], Giovanni Castellazzi[1], Stefano de Miranda[1], Gabriele Milani[2]*

[1] Department of Civil, Chemical, Environmental, and Materials Engineering (DICAM), University of Bologna, Viale del Risorgimento 2, Bologna 40136, Italy

[2] Department of Architecture, Built Environment and Construction Engineering, Technical University of Milan, Piazza Leonardo Da Vinci, Milan 20133, Italy

*corresponding author: gabriele.milani@polimi.it

ABSTRACT

In this paper, a two-step automated procedure based on adaptive limit and pushover analyses is developed for the seismic assessment of masonry structures. Inspired by an akin procedure previously developed by the authors for the out-of-plane behaviour, the procedure herein presented is extended to in-plane and combined in- and out-of-plane loading conditions, accounting also for the effect of masonry crushing failure. In the first step, an upper-bound adaptive limit analysis tool is used to predict the collapse mechanism (and the corresponding multiplier) of the structure given a certain loading condition. A novel ad-hoc routine is then developed and utilized for the automatic import of the collapse mechanism geometry of any complexity into a solid model ready to be used in a finite element framework. In the second step, cohesive-frictional contact-based interfaces are automatically inserted in the cracks of the collapse mechanism formerly obtained, and a pushover analysis is conducted to investigate the load-displacement response of the structure. A series of parametric analyses are conducted to highlight the effect of different mechanical assumptions. Finally, the effectiveness of the procedure proposed is shown on a full-scale masonry building case study.

Keywords: Unreinforced masonry; Limit analysis; Collapse mechanisms; Load-displacement curve; Softening behaviour; Pushover analysis

Nomenclature

$\mathbf{A}$	matrix of geometric constraints
$\mathbf{B}$	matrix containing the normal unit vectors for the linearized 3D failure domain
$\mathbf{c}$	vector of internal dissipated power
c	cohesion of the contact shear response
D	scalar damage variable for the contact behaviour
d_c	compressive scalar damage variable for the plastic-damage model
d_t	tensile scalar damage variable the plastic-damage model
E	Young's modulus of the material
E_0	initial Young's modulus of the material
f	three-dimensional failure domain
f_{b0}	biaxial initial compressive strength
f_{c0}	uniaxial initial compressive strength
f_c	compressive strength
f_s	contact shear strength
f_t	contact tensile strength
G_f	fracture energy
K_{nn}	contact cohesive stiffness in normal direction
K_{ss}	contact cohesive stiffness in shear direction
n	normal unit vector to the interface
$\dot{\mathbf{p}}$	non-negative plastic multiplier
$\mathbf{q}_0$	dead-load vector
$\mathbf{q}$	live-load vector
$\mathbf{R}$	matrix containing the local reference systems
s	first tangential unit vector to the interface
t	second tangential unit vector to the interface
$\tan\phi$	initial friction of the contact shear response
u	contact normal displacement
u_0	separation at the limit of the linear elastic behaviour in tension
u_k	ultimate separation of the cohesive behaviour
u_{MAX}	maximum separation ever experienced by the contact point
$\dot{\mathbf{u}}$	velocity vector
$\Delta\dot{\mathbf{u}}$	velocity jumps in the external reference system
w	material density
δ	contact tangential slip
δ_0	slip at the limit of the linear elastic behaviour in shear
δ_k	ultimate slip of the cohesive behaviour
δ_{MAX}	maximum slip ever experienced by the contact point
ε_c	uniaxial compressive strain
ε_t	uniaxial tensile strain
ε_c^p	uniaxial compressive plastic strain
ε_t^p	uniaxial tensile plastic strain
ϵ	smoothing constant
ν	Poisson's coefficient
ρ	shape constant
$\boldsymbol{\sigma}$	vector of stress in the local reference system
σ	contact normal stress
σ_c	uniaxial compression
σ_t	uniaxial tension
λ	live-load multiplier
μ	residual friction
τ	contact shear stress
φ	friction angle used in the limit analysis
ψ	dilatancy angle of the quasi-brittle material

1 Introduction

The prediction of the seismic collapse and near-collapse behaviour of existing and historical masonry structures is a burning issue in the scientific community. Indeed, many modelling strategies have been developed in the last decades [1] to overcome the several challenges which characterize these structures, e.g. highly nonlinear mechanics of masonry, anisotropic masonry behaviour, complex geometries of masonry structures, etc.

Two main analysis approaches can be distinguished for masonry structures [2]: (i) limit analysis-based and (ii) incremental-evolutive approaches.

Limit analysis-based approaches (i) are well-known reliable tools for the investigation of the collapse mechanism and collapse multiplier of masonry structures. Beginning from the research work proposed by Heyman [3], many approaches have been developed using lower bound [4, 5, 6, 7, 8] and upper bound [9, 10, 11, 12] limit analysis formulations. Within a finite element method (FEM) framework, upper bound limit analysis-based tools are generally preferred [13, 14, 15], following the hypothesis of energy dissipation on interfaces between elements (firstly developed in [16]). These tools have also been lately optimized by using adaptive mesh refinements to boost the computations [17, 18, 19]. However, limit analysis-based approaches typically do not provide information about the structural load-displacement response, although this would be essential in displacement-based seismic verification procedures, which are extensively used in practice and seem to be preferred rather than force-based procedures [20].

Incremental-evolutive approaches (ii) are widely utilized tools for the step-by-step investigation of the structural equilibrium in nonlinear iterative analysis frameworks, often used in pushover analyses for the seismic assessment of masonry structures [21]. These approaches can be used within three modelling strategies for masonry structures:

- Macro-element models or simplified models in general (see e.g. [22, 23, 24, 25, 26, 27]), widely used in common engineering practice due to their simplicity, although typically limited to ordinary buildings and not applicable for complex monumental structures;
- Block-based models (see e.g. [28, 29, 30, 9, 31, 32]), where masonry is block-by-block modelled (typically into Finite Elements) and the interaction between blocks can be accounted for through various formulations. Although potentially highly accurate, their main drawback could be represented by the large computational demand;
- Continuum models (see e.g. [33, 34, 35, 36]), where masonry is modelled through a deformable continuum and the constitutive law can be defined directly or through a multi-scale framework. These models, although interesting and potentially very effective, could be computationally expensive or could find difficulties in representing the post-peak response due to convergence issues, as well as the collapse mechanism predicted could be, in general, not fully clear [37].
- Discrete element models -or restricting the family of the approaches proposed, Distinct Element Methods DEMs- (as for instance those presented in [38, 39, 40, 41, 42, 43, 44, 45, 46, 46] without being exhaustive) where masonry is modelled with rigid or elastic blocks and all non-linearity is lumped on joints typically assumed with a cohesive frictional behaviour [46, 45]. Such approach is conceived mainly for Non Linear Dynamic Analyses [47, 48, 49] computations NLDAs but performs in a quite reasonable manner both for pushover and non linear analyses in general, in presence also of foundation settlements, albeit requiring typically huge computational efforts. There are obviously other important drawbacks that cannot be summarized in few words in this introduction, but it is interesting to point out how they have recently inspired the implementation of FEM combined with DEM for large scale analyses (see for instance [50, 51, 52]).

Accordingly, both limit analysis-based and incremental-evolutive approaches present either advantages or disadvantages, and their coupling would represent a favourable solution. The research carried out by part of the authors in [53] represented a fist attempt to couple limit analysis-based solutions to displacement-based evolutive analysis strategies for out-of-plane-loaded masonry structures. Particularly, in [53] the collapse mechanism deduced by genetic algorithm-based adaptive limit analysis has been used in a pushover-based framework using two different approaches to introduce nonlinearities in the model. The first one considered

3D plastic damaging strips governed by a nonlinear continuum constitutive law, while the second exploited zero-thickness contact-based interfaces governed by a cohesive-frictional contact behaviour. Both the approaches showed good performances in simulating the out-of-plane behaviour of masonry structures, with the latter showing a lower computational demand.

In this paper, a two-step automated procedure based on adaptive limit and pushover analyses is developed for the seismic assessment of masonry structures. This approach extends the one developed in [53] to in-plane and combined in- and out-of-plane loading conditions, accounting also for the effect of masonry crushing failure. Accordingly, the procedure herein presented represents a general method for the seismic assessment of historic and ordinary buildings of any geometrical complexity. In other words, the two-step procedure herein presented becomes general as it can deal with in-plane, out-of-plane, and both combined failure modes, accounting also for crushing failures which may appear substantial in many practical cases.

In the first step, an upper-bound adaptive limit analysis tool is used to predict the collapse mechanism (and the corresponding multiplier) of the structure given a certain loading condition. A novel ad-hoc routine is then developed and utilized for the automatic import of the collapse mechanism geometry of any complexity into a solid model ready to be used in a finite element framework.

In the second step, cohesive-frictional contact-based interfaces are automatically inserted in the cracks of the collapse mechanism formerly obtained, and a pushover analysis is conducted to investigate the load-displacement response of the structure. Accordingly, the pushover curves of a masonry structure can be obtained and used in most verification procedures, see e.g. [54], for its seismic assessment. A series of parametric analyses are conducted to highlight the effect of different mechanical assumptions, e.g. continuum plastic-damage behaviour to account for crushing. Finally, the effectiveness of the procedure proposed is evaluated on a full-scale masonry building case study.

The paper is organized as follows. Section 2 presents the main features of the two-step analysis framework herein proposed. Section 3 shows a set of parametric analyses carried out on an in-plane loaded windowed panel, as well as the validation of the proposed approach. Section 4 shows the effectiveness of the two-step procedure on a full-scale masonry building case study. Finally, Section 5 highlights the conclusions of this research work.

2 Two-step analysis framework

A graphical overview of the two-step analysis procedure developed in this paper is represented in Fig. 1. Given a structure and its material properties, an upper-bound adaptive limit analysis is carried out for a certain loading condition (Section 2.1). The outcomes of this first step (Step 1 in Fig. 1) consist in the geometry of the collapse mechanism and its collapse multiplier, which can be expressed in terms of maximum base shear.

The geometry of the collapse mechanism is then processed by an ad-hoc routine that disassembles it in elementary parts, removes superfluous information, and returns a set of polylines which can be easily exploited to generate a 3D model in a CAD environment (Routine 1-to-2 in Fig. 1), to which favourable adjustments can be applied in order to generate a structure geometry representation which is consistent with the requirements of a FE software. More details about the Routine 1-to-2 are given in Section 2.2.

The solid CAD geometry is finally imported in a FE software in Step 2 (Fig. 1), where zero-thickness contact-based surfaces (Section 2.3) are automatically inserted in correspondence of the fissures derived through the adaptive limit analysis collapse mechanism. Once constraints and loading conditions (coherent with those adopted in Step 1) are defined by the user, as well as the mechanical properties assumed in agreement with those adopted in Step 1, a pushover analysis is carried out to derive the load-displacement response. Eventually, the maximum base shear derived through the two strategies is compared to assess the consistency of the present approach.

Concerning the geometry management along with the procedure (Fig. 1), it is worth mentioning that the masonry structure is initially modelled through planar NURBS surfaces. Then, each surface is converted into a 3D element through the assignment of the thickness and 2D interfaces are defined between adjacent elements in Step 1. In Step 2, 3D solid FEs are used to model the portions of the structure and 2D contact surfaces define the interaction between the adjacent portions.

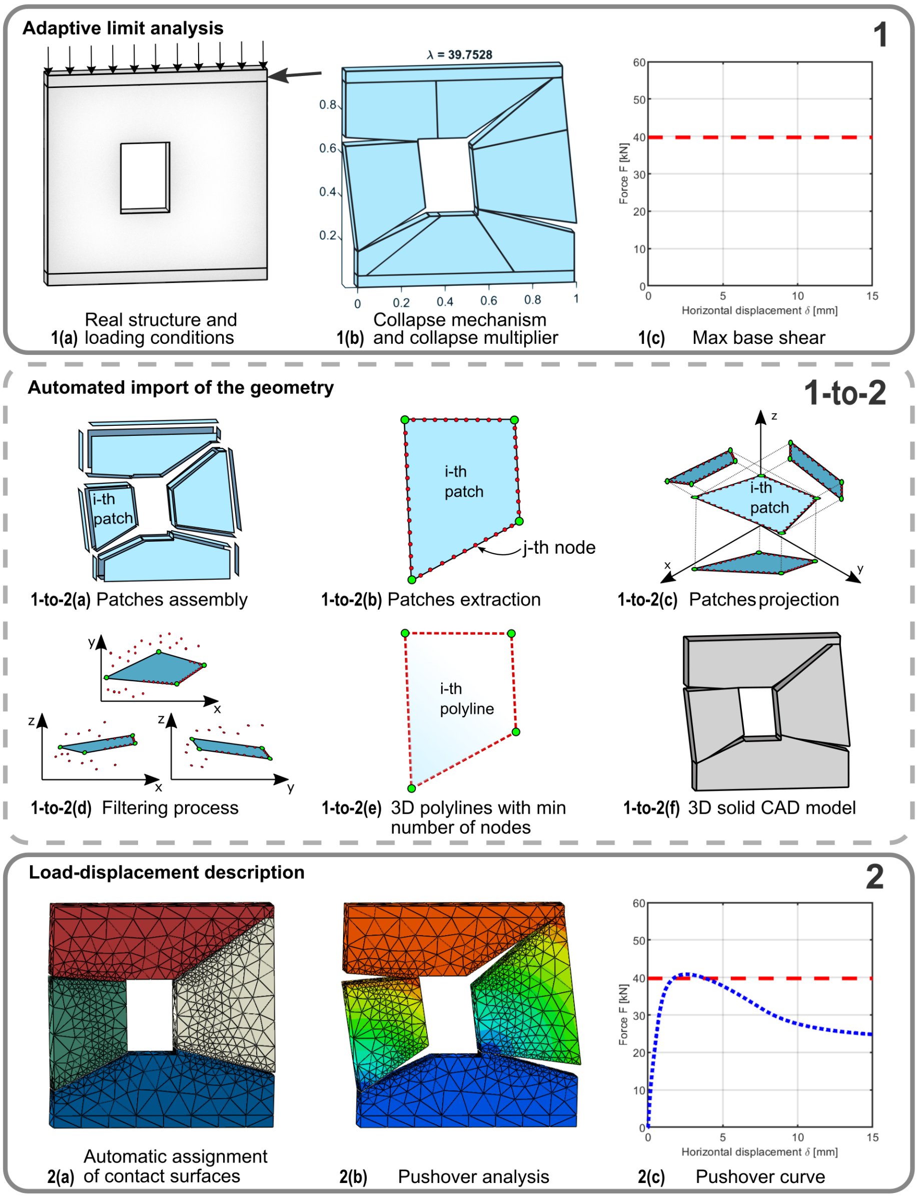

Fig. 1 - Two-step analysis procedure.

2.1 Adaptive NURBS-based limit analysis

The first step of the procedure consists of an adaptive kinematic limit analysis based on the use of NURBS three-dimensional (3D) finite elements. The first presentation of this method, initially conceived for the limit analysis of masonry vaults, is reported in [18].

The masonry structure is firstly modelled into the Rhinoceros environment by using NURBS curved or planar surfaces. A NURBS surface (Non-Uniform Rational Bezier Spline, [55]) is a parametric surface whose basis functions are piecewise polynomial rational functions obtained starting from the traditional spline basis function. They are widely used in the representation of curved geometries. In this approach, NURBS properties are used to both represent exactly curved geometries and facilitate mesh adaptation procedures.

The NURBS model of the whole masonry structure is imported within MATLAB as IGES standard file. Each surface is here converted into a 3D element once that a thickness value has been assigned to it. Each element is supposed rigid and infinitely resistant. Moreover, a mesh composed of few elements can be obtained by considering each initial surface as the union of trimmed surfaces. By applying some simple subdivision algorithms directly within MATLAB, an assembly of rigid blocks can be defined. A kinematic limit analysis is then applied.

Given a configuration of loads $[\mathbf{q}_0, \lambda\mathbf{q}]$, in which $\mathbf{q}_0$ are the permanent loads and $\mathbf{q}$ is a live-load depending on a multiplier λ, a mechanism involving the few rigid elements composing the initial mesh can be identified by solving a standard linear programming problem. The mechanism is described by a velocity field $\dot{\mathbf{u}}$ that contains the six velocity components (three translational and three rotational) of each centroid and presents discontinuities (i.e. velocity jumps) at the boundaries of each portion. To properly quantify the velocity jumps, two-dimensional (2D) rigid-plastic interfaces are defined at the common boundaries between adjacent elements. Each interface is discretized through points to which the associative flow rule is imposed:

$$\mathbf{R}\Delta\dot{\mathbf{u}} = \left(\dot{\mathbf{p}}^T \frac{\partial f}{\partial \boldsymbol{\sigma}}\right)^T \tag{1}$$

where $\Delta\dot{\mathbf{u}}$ are the velocity jumps defined in the external reference system, the transformation matrix $\mathbf{R}$ contains the local reference systems nst (in which n, s, and t are respectively the normal and the two tangential directions) on each point, $\dot{\mathbf{p}}$ are the non-negative plastic multipliers, $\boldsymbol{\sigma} = [\sigma_{nn}, \tau_{ns}, \tau_{nt}]^T$ is the local stress vector, and f is the linearized three-dimensional failure surface assigned to masonry.

The surface f represents a Mohr-Coulomb failure criterion expressed in the local reference system. A tension cut-off and a linear cap in compression are included to limit respectively the maximum tensile strength f_t (usually equal to $c/tan(\varphi)$ within a standard Mohr-Coulomb frictional law, where c is the cohesion and φ is the friction angle) and the maximum compression strength f_c that masonry can undergo.

The linear programming problem that solves the kinematic formulation is summarized as follows:

$$\min\left\{\lambda = \frac{\mathbf{c}\dot{\mathbf{p}} - \boldsymbol{q}_0\dot{\mathbf{u}}}{\mathbf{q}\dot{\mathbf{u}}}\right\} \text{ such that } \begin{cases} \mathbf{A}\dot{\mathbf{u}} = \mathbf{0} & (a) \\ \mathbf{R}\Delta\dot{\mathbf{u}} - \mathbf{B}\dot{\mathbf{p}} = \mathbf{0} & (b) \\ \mathbf{q}\dot{\mathbf{u}} = 1 & (c) \\ \dot{\mathbf{p}} \geq \mathbf{0} & (d) \end{cases} \tag{2}$$

where: λ is the kinematic multiplier deduced by applying the Principle of Virtual Powers, (a) are the geometric constraints, (b) represent the imposition of the associated plastic flow rule at interfaces, (c) is the normalization of the power dissipated by live-loads for a unitary load multiplier, and (d) is the constraint of non-negativity of the plastic multipliers. A mechanism is thus obtained.

However, the use of a reduced number of macro-elements makes the problem highly mesh-dependent. According to the upper bound theorem of limit analysis, the collapse load multiplier is the minimum of the kinematic load multipliers and it is associated to the real collapse mechanism, which is properly identified only if the interfaces between adjacent elements coincide with the real position of fracture lines. Therefore, a procedure of mesh adaptation must be applied. The initial mesh is iteratively adjusted until the global minimum of the kinematic load multipliers is found. For this operation, a meta-heuristic approach is used. Among the several available meta-heuristic algorithms (Genetic Algorithm, Particle Swarm Optimization, Firefly Algorithm, and Prey-Predator Algorithm [56]), a Genetic Algorithm (GA) [57] with crossover through random binary vectors is here applied.

Within the GA, a population of random individuals is generated at the first iteration. Each individual consists of a vector which contains the information (usually, the nodal displacements) for the adjustments relative to the initial mesh, thus defining a possible varied mesh. The evaluation of the kinematic load multiplier (Eq. 2) is the objective function. For each individual, the objective function is evaluated and that associated with the minimum value of the objective function is the best individual. Then, a crossover procedure is used to combine individuals in pairs and generate a new population. In particular, for each couple of individual vectors a random binary vector is used to swap their genes (nodal displacements) and generate two new individuals. Random changes can be then inserted in new individuals to preserve diversity and avoid premature convergences around local minima. Several numerical strategies can be followed in this step, for the sake of simplicity the reader is referred to [57]. Once the new population has been defined, a new iteration starts. The procedure stops when the minimum function value achieves the convergence. The best individual of the last iteration represents the mesh associated with the real collapse mechanism and the collapse load multiplier. For a theoretical dissertation and applications about this method, we refer to e.g [18] [19] [58].

A final consideration is reported. Since the final mechanism is identified according to the fundamental hypotheses of limit analysis, an associative behaviour in shear is considered for masonry. Dilatancy effects are thus observed when shear failures occur. To avoid dilatancy and obtain pure-sliding collapses in shear, a non-associative behaviour can be represented by using the sequential linear programming procedure described in detail in [59].

2.2 Automated import of the geometry

In this section, the automated import of geometry from Step 1 to Step 2 (Routine 1-to-2 in Fig. 1) herein developed to overcome the drawback of manually recreating the geometry of the collapse mechanism is briefly described. The interested reader is referred to Appendix A for further details.

It appears clear, indeed, that more complex is the collapse mechanism to be investigated, the more time would be needed to manually adapt the imported geometry to perform the pushover analysis. Furthermore, it has to be pointed out that the automatization of this task substantially minimizes the human error, which could have a significant impact especially when dealing with large and complex geometries.

The starting point (i.e. the outcome of Step 1) consists in a file where the collapse mechanism is represented by means of an assembly of patches, namely graphical objects used to model 3D entities, which are in turn defined by the coordinates of their nodes (Fig. 1). The geometry of every portion of the mechanism is described independently (e.g. the surface between two structural portions in contact is described by two identical overlapping patches), and a filtering process is implemented to avoid redundant nodes (see Fig. 2 and Appendix A), using as filtering criterion two values of tolerance called in the Appendix toll1 and tool2.

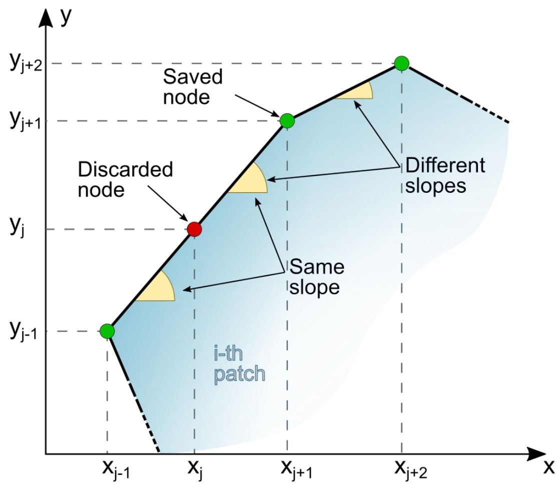

Fig. 2 - Graphical interpretation of the filtering algorithm.

Accordingly, the description of the mechanism can be utilized to generate a 3D model in any CAD environment, which is a useful middle step that allows to apply, if needed, practical adjustments before it is imported into a finite element software capable of importing the most common 3D file formats. Routine 1-to-2 takes in input a figure file and returns another file that automatically generates the solid geometry in a CAD environment (Fig. 3).

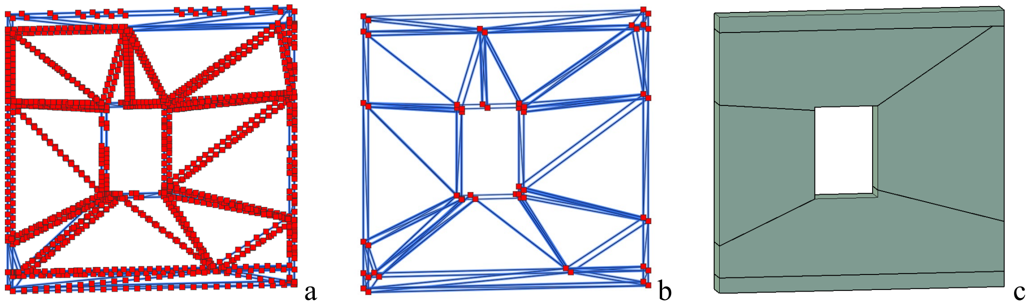

Fig. 3 – Collapse mechanism geometry in the CAD environment: (a) polylines model generated without applying the filtering process, (b) polylines model generated using the filtering process, (c) solid model.

2.3 Load-displacement description

Step 2 aims at the load-displacement description of the collapse mechanism (Fig. 1). To this scope, an incremental-evolutive approach is employed, and the interaction between the portions composing the collapse mechanism is idealized through a contact-based formulation with friction and cohesion (Fig. 4).

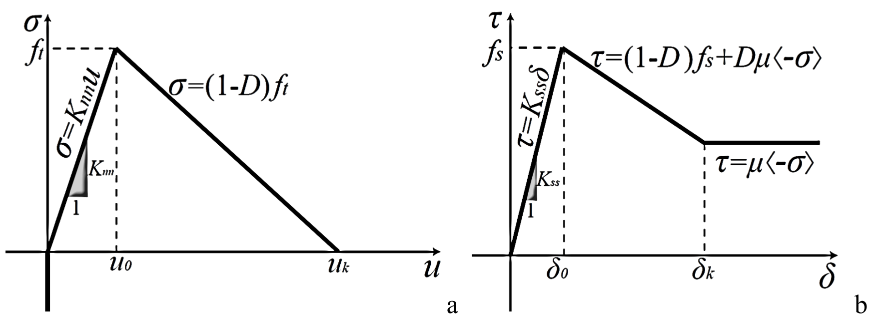

Fig. 4 – Tensile (a) and shear (b) contact behaviour between portions.

Particularly, the tensile and shear contact stresses are computed as:

$$\sigma = \begin{cases} K_{nn}u, & \text{with } \sigma \geq 0 \\ \text{Lagrange contact constraint}, & \text{with } \sigma < 0 \end{cases}, \qquad \tau = K_{ss}\delta \tag{3}$$

where σ is the normal contact stress positive in tension, τ is the shear contact stress, u is the normal displacement between portions, δ is the tangential slip between portions, K_{nn} is the normal cohesive stiffness and K_{ss} is the shear cohesive stiffness in shear. The setting of these stiffness values in block-based models is discussed e.g. in [60]. It has to be pointed out that, in this work, the values of K_{nn} and K_{ss} are assumed to be compatible with the elastic properties of the portions in contact, avoiding excessive localized deformations at the contact surfaces if compared to the overall structural response. Failure in contact point occurs when the contact stress reaches a Mohr-Coulomb-type failure surface with tension cut-off. Such failure criterion, which has been implemented in Abaqus [61] through an automatic user-defined subroutine, can be expressed as:

$$\max\left\{\frac{\langle\sigma\rangle}{f_t}, \frac{|\tau|}{f_s(\sigma)}\right\} = 1, \tag{4}$$

where $\langle\sigma\rangle = (|\sigma| + \sigma)/2$ indicates that merely compression does not cause contact failure, f_t is the tensile strength and f_s is the shear strength described as:

$$f_s(\sigma) = c - \sigma \tan\phi, \tag{5}$$

being c the shear cohesion and $\tan\phi$ the initial friction. In a contact point, accordingly, the maximum normal and shear stresses are defined as:

$$\sigma = \begin{cases} (1-D)f_t, \text{ with } u < u_k \\ 0, \text{ with } u \geq u_k \end{cases}, \qquad \tau = \begin{cases} (1-D)f_s(\sigma) + D\mu\langle-\sigma\rangle, \text{ with } \delta < \delta_k \\ \mu\langle-\sigma\rangle, \text{ with } \delta \geq \delta_k \end{cases} \tag{6}$$

where μ is the residual friction, u_k and δ_k are the ultimate separation and the ultimate slip of the cohesive behaviour, respectively, and D is the contact damage, which is assumed to evolve linearly along with displacements as:

$$D = \begin{cases} 0, & \text{with } u \leq u_0 \text{ and } \delta \leq \delta_0 \\ \max\begin{cases} \dfrac{u_{MAX} - u_0}{u_k - u_0}, & \text{with } u_0 < u < u_k \\ \dfrac{\delta_{MAX} - \delta_0}{\delta_k - \delta_0}, & \text{with } \delta_0 < \delta < \delta_k \end{cases} \\ 1, & \text{with } u \geq u_k \text{ or } \delta \geq \delta_k \end{cases}. \tag{7}$$

being u_0 and δ_0 the separation and the slip at the elastic limit in tension and shear, respectively, and u_{MAX} and δ_{MAX} the maximum separation and the maximum slip ever experienced by the contact point, respectively. In the following, the assumption $\phi = \tan^{-1}(\mu) = 30°$ is considered, being a typical value for masonry [53]. Furthermore, it should be noted that u_k can be easily deduced from the value of contact fracture energy G_f and the assumption of $u_k = \delta_k$ is also adopted for simplicity.

The potential effects of masonry crushing failure can be accounted for in the portions of the collapse mechanism through a nonlinear continuum plastic-damage constitutive law. Particularly, the standard concrete damaged plasticity (CDP) model implemented in Abaqus [61] has been herein considered. The interested reader is referred to Appendix B for details about the CDP model and its setting.

The resulting model is then considered in a pushover-based framework (Fig. 1) to predict the load-displacement description (i.e. pushover curve) of the structure.

3 Preliminary analyses

3.1 Benchmark description and adaptive limit analysis

The first benchmark consists of a windowed panel tested in [62]. The panel (see Fig. 5) was composed of 18 courses of bricks 210×52×100 mm^3 and mortar joints 10 mm thick, resulting in the overall width and height respectively equal to 990 mm and 1000 mm. A central opening has been realized. As permanent load, a vertical pre-compression of 0.3 MPa was applied and maintained constant during the test. The test was conducted by applying a horizontal load by means of a steel beam fixed at the top of the wall. Previous homogenized limit analysis and non-linear analysis performed on this benchmark were presented in [63].

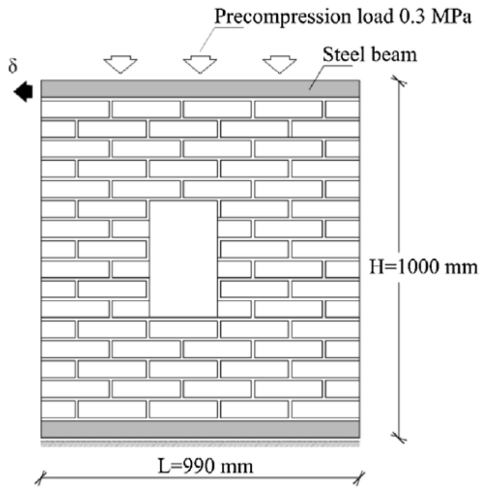

Fig. 5 - Masonry windowed panel: geometry and load conditions.

The adaptive limit analysis has been applied to this panel. An additional rigid element has been added to the model to represent the steel beam. The live-load is modeled through a horizontal pointed load equal to $\lambda\cdot 1$ kN applied at the top. A tensile strength of 0.25 MPa and a compression strength of 10.5 MPa have been assigned coherently with [63] (see also Table 1 for reference parameters); as regards the shear behavior, a fictitious shear resistance equal to 0.5 MPa has been used to avoid unrealistic pure sliding failures.

The NURBS model of the masonry panel has been subdivided into rigid elements by following two initial mesh separately, one composed of quadrangular elements and the second one composed of triangular elements as depicted in Fig. 6a. In both the cases, the mesh adaptation is applied by moving the nodes from their initial position. Considering that nodes at the external boundaries are constrained to be moved along their boundary, both the mesh adjustments are described by a total of 16 parameters. A total number of 80 individuals and 50 maximum generations have been used. As it can be noted in Fig. 6b, the best solution is found after few iterations with both the mesh. A final collapse load of 39.75 kN has been found. This result is in good agreement with the previous ones reported in [63]. The final collapse mechanism obtained through quadrangular elements is depicted in Fig. 6c. Considering the lower number of elements with reference to the mesh by triangular elements, the next pushover analysis has been conducted starting from this mechanism.

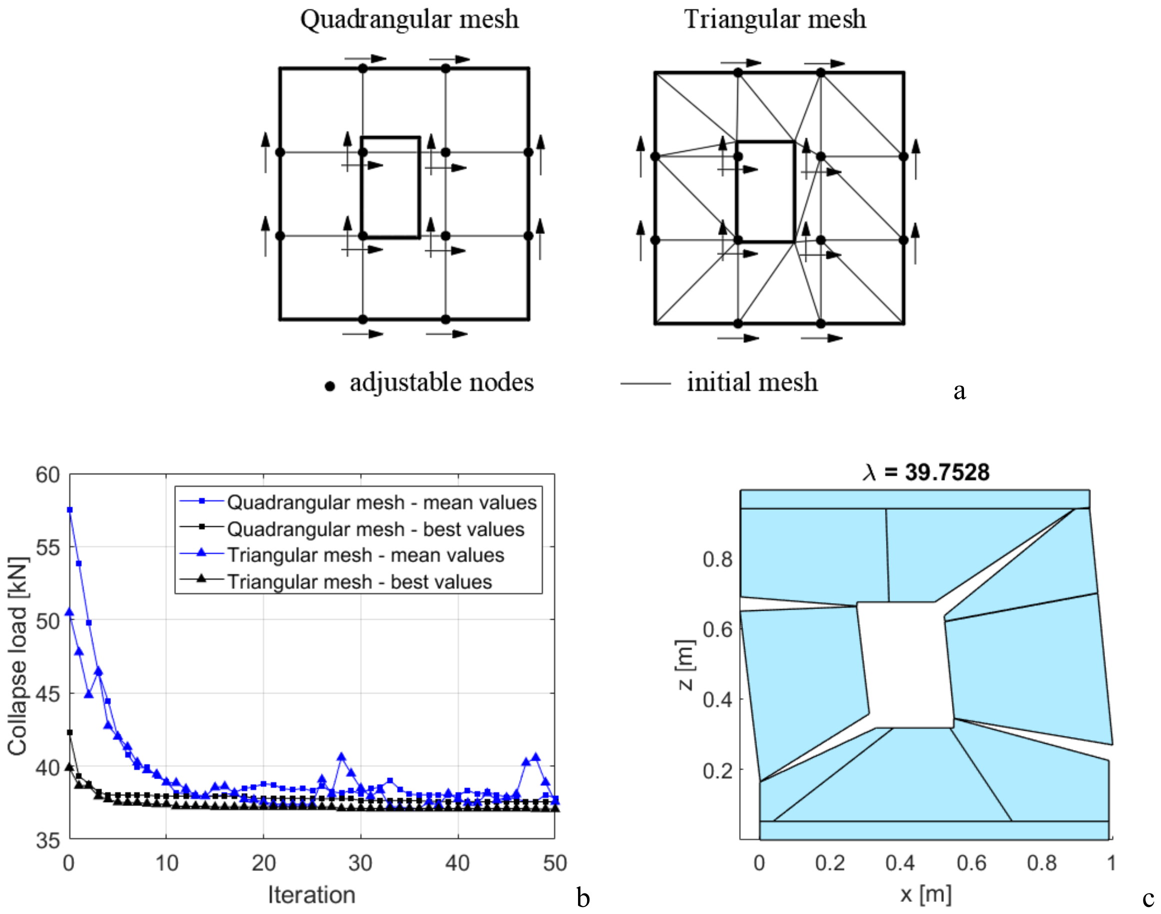

Fig. 6 – Adaptive limit analysis of the windowed panel: (a) two different initial mesh adopted, (b) GA-convergence diagrams, and (c) collapse mechanism obtained through the initial quadrangular mesh.

3.2 Parametric analyses

In this section, the results of several parametric analyses carried out to evaluate the influence of the adopted parameters on the load-displacement solution are shown and discussed. The mechanical properties listed in Table 1 are taken as reference values (i.e. for a set of parametric analyses executed to study e.g. the influence of G_f, only this value will change in a predetermined range, while the remaining parameters will be kept equal to those specified in Table 1).

Table 1. Windowed panel reference parameters.

Material density	w	$[kg/m^3]$	1900
Material Young's modulus	E	$[MPa]$	8000
Material Poisson's coefficient	υ	$[-]$	0.2
Contact cohesion	c	$[MPa]$	0.5
Contact tensile strength	f_t	$[MPa]$	0.25
Contact normal cohesive stiffness	K_{nn}	$[N/m^3]$	$2{\cdot}10^9$
Contact shear cohesive stiffness	K_{ss}	$[N/m^3]$	10^{10}
Contact fracture energy	G_f	$[N/m]$	5000

The influence of mesh refinement has been firstly investigated. The models with different mesh sizes and the results in terms of pushover curves are shown in Fig. 7. According to the outcomes exposed in the graph, it can be noted that mesh refinement does not appear to particularly affect the results, which can be a big advantage in terms of computational effort needed to perform the analyses. Anyway, a good compromise between accuracy and computational effort can be achieved providing a mesh refinement near the contact surfaces. Accordingly, all the analyses exposed in the following have been conducted on models which employ the optimized mesh shown in Fig. 7e.

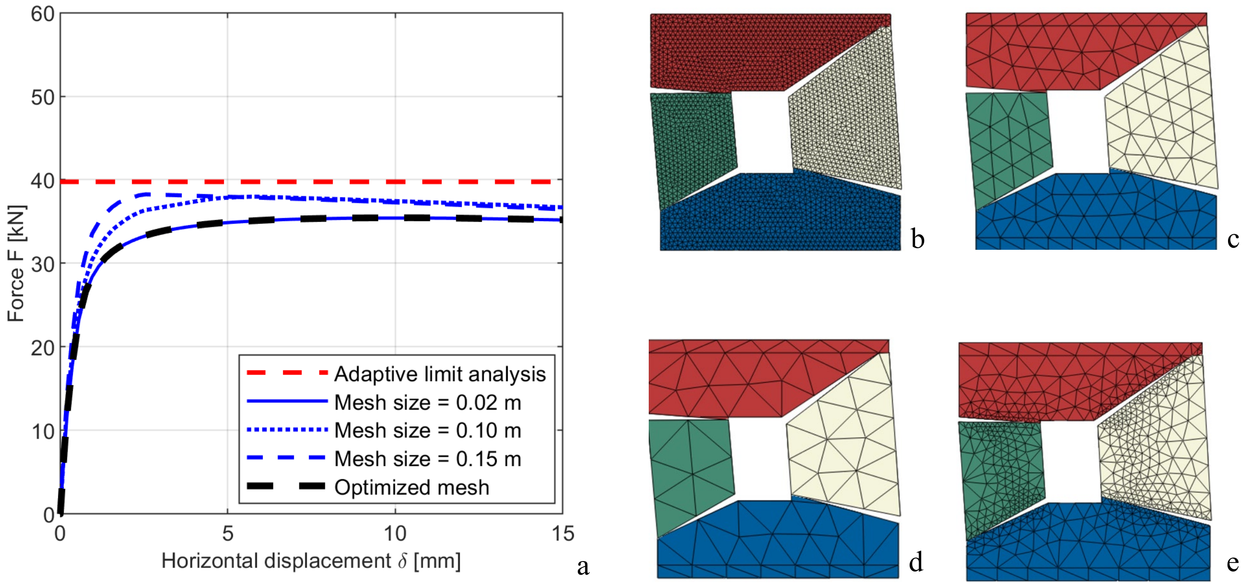

Fig. 7 – Mesh influence, approximate global size of: (a) 0.02m, (b) 0.1m, (c) 0.15m, (d) optimized.

In [53], the numerical procedure has been applied to out-of-plane loaded structures for which the compressive damage was not considered as, in general, it has a negligible influence on the structural response. In an in-plane loaded structure, compressive stress is more likely to reach the compressive strength of the material and crushing damage cannot just be disregarded as done for the out-of-plane case. Accordingly, crushing failure has been accounted for by means of the CDP model (Appendix B). The specimens tested experimentally in [62] were characterized by a compressive strength $f_c = 10.5\ MPa$, and, hence, this value has been firstly considered. As shown in Fig. 8, compressive failure appears to be not significant and, indeed, its pushover curve does not noticeably differ from the one with infinite compressive strength. To highlight the potential impact of crushing, a lower value of compressive strength $f_c = 2.5\ MPa$ has been considered (for the complete set of CDP parameters see Appendix B). As can be noted, for this benchmark crushing failure slightly influences the structural response, mostly affecting the post-peak response (Fig. 8).

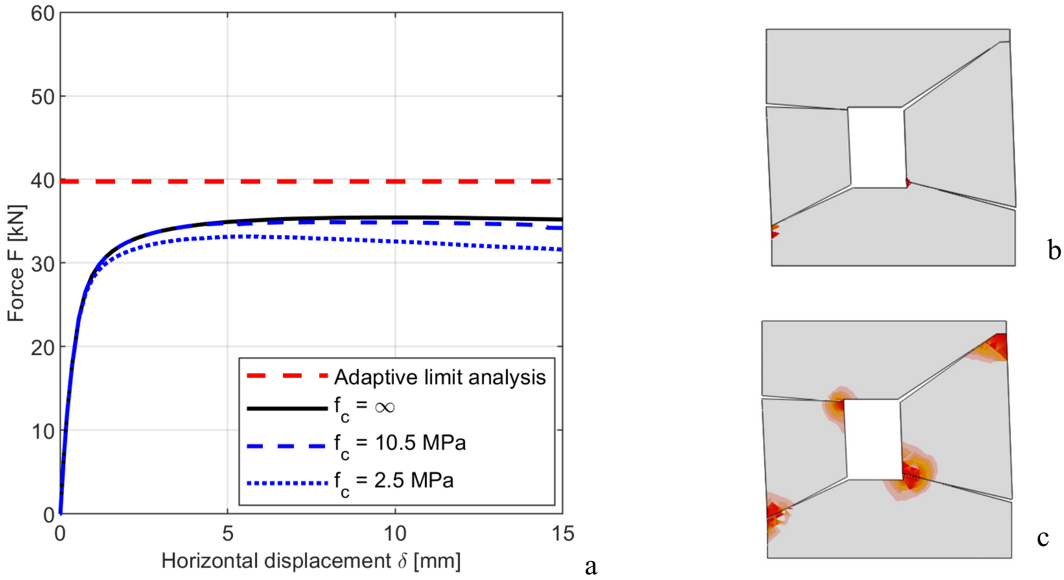

Fig. 8 - Parametric analysis - Influence of the compressive strength on the pushover curves (a). Compressive damage pattern on a model with: (b) fc=10.5MPa, (c) fc=2.5MPa.

Then, the influence of normal cohesive stiffnesses on the overall response has been parametrically evaluated (Fig. 9). As it can be noted, the normal contact cohesive stiffness primarily influences the slope of the linear branch of the pushover curve, whereas its influence on the peak shear load appears very limited.

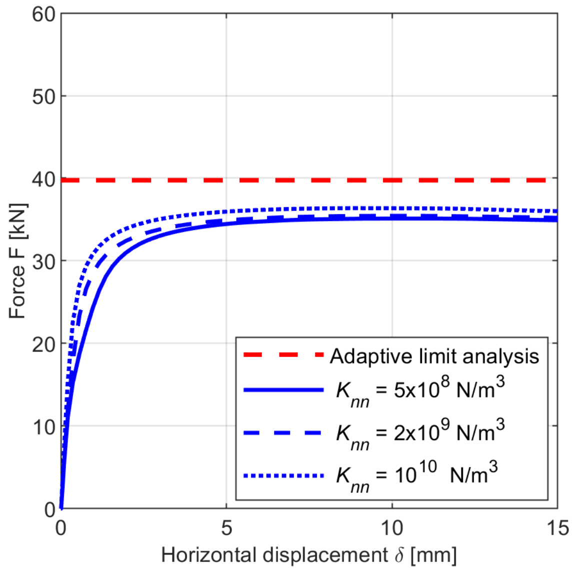

Fig. 9 - Parametric analysis - Influence of the normal contact stiffness.

Another aspect that has been investigated is the influence of the fracture energy G_f. Referring to Fig. 10a, it can be observed that its influence on the structural response is significant. Indeed, the post-peak response of the structure goes from having a softening trend to a ductile one for increasing values of G_f. Particularly, the limit case with $G_f = 10000\, N/m$ (i.e. an unrealistic value) shows a load-displacement response without softening. It has to be pointed out that the maximum base shear obtained in this case results slightly lower from that obtained through upper-bound adaptive limit analysis. This appears reasonable given that the limit analysis gives an upper-bound solution and the deformability of the system considered in Step 2 can have a slight impact on the peak shear load (see e.g. Fig. 9).

The pushover-based step (Step 2) can be also performed accounting for the orthotropic nature of the masonry material. Indeed, considering a reference system with the x axis horizontal, parallel to the bed joints of a brick masonry specimen, and the y axis in the vertical direction, we can refer to f_{ty} as the masonry tensile strength when the specimen is subjected to traction in the vertical direction, while f_{tx} represents the masonry tensile strength when traction forces act in the horizontal direction. Likewise, G_{fy} and G_{fx} are respectively the associated fracture energies, and c_y and c_x the respective cohesion values. In order to consider the orthotropic behaviour, the following expressions are then introduced:

$$\begin{aligned} f_t(\theta) &= f_{tx} \cdot \big(sin(\theta)\big)^2 + f_{ty} \cdot (\cos(\theta))^2, \\ G_f(\theta) &= G_{fx} \cdot \big(sin(\theta)\big)^2 + G_{fy} \cdot (cos(\theta))^2, \\ c(\theta) &= c_x \cdot \big(sin(\theta)\big)^2 + c_y \cdot (\cos(\theta))^2, \end{aligned} \tag{8}$$

where θ denotes the angle between the x axis and a line parallel to the contact surface. Moreover, it is assumed, in general agreement with consolidated homogenization literature comparing horizontal and vertical inelastic properties (see for instance [64] [65]) that:

$$f_{tx} = 6 \cdot f_{ty}; \qquad G_{fx} = 10 \cdot G_{fy}; \qquad c_x = 6 \cdot c_y \tag{9}$$

with f_{ty}, G_{fy}, and c_y taken equal to the values of f_t, G_f, and c in Table 1. Particularly, the relations in (9) are assumed as they represent the maximum ratio between horizontal and vertical masonry properties observed in [66], that we adopted also with the aim to maximize the differences with the constant properties case and check the range of expected solutions. The influence of fracture energy in the pushover curves has then been studied for the orthotropic material (Fig. 10b), i.e. considering the contact mechanical properties varying along with θ according to (8) and (9). As can be noted, higher values of peak base shear are observed, obtaining a more significant softening behaviour in the cases with low fracture energy. In this case, higher or slightly higher load values with respect to the limit analysis solution are observed (Fig. 10b). Particularly, the curve in Fig. 10b characterized by $G_{fy} = 500\,N/m$ and $G_{fx} = 5000\,N/m$ is assumed in the following as reference solution, since it considers the orthotropic nature of masonry and employs values of fracture energy typically assumed in masonry structures.

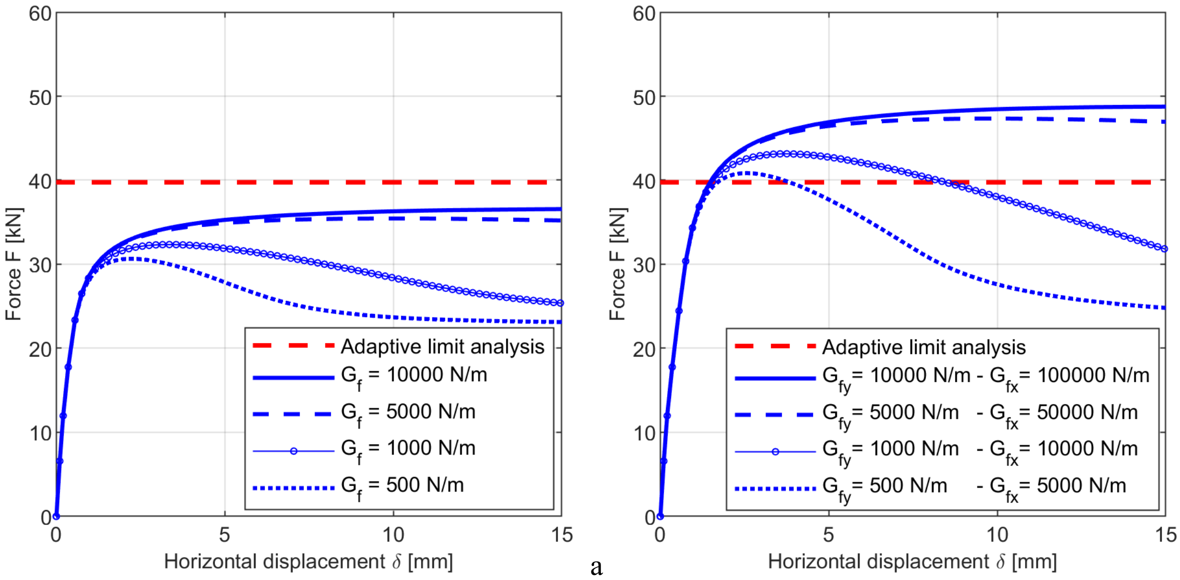

a b

Fig. 10 - Parametric analyses - Influence of the fracture energy: (a) constant contact mechanical properties, (b) contact mechanical properties depend on the surface slant.

3.3 Validation

The reference solution obtained in the previous section is compared in Fig. 11 with the results of an experimental campaign executed on a windowed shear panel (two replicates) by Raijmakers and Vermeltfoort in [62], and with a series of pushover curves obtained through other numerical approaches. In detail, these are derived through the following approaches: a micromodel with interface elements used as potential damage planes described by Lourenço and Rots in [60], a continuum model with a mechanical behaviour described by an implicit orthotropic model based on continuum damage mechanics by Pelà [36], an in-plane stress state continuum model with orthotropic failure criterion presented by Bilko and Malyszko in [67], and a quadratic programming (QP)-based model composed by rigid triangular elements interacting through zero-thickness nonlinear interfaces, investigated by Milani in [63] for three different meshes. Furthermore, the maximum base shear obtained with the adaptive limit analysis procedure in Section 3.1 is added, see the horizontal dotted line.

Inspecting Fig. 11, it can be observed that the two-step procedure herein proposed shows favourable results. Indeed, the outcome of the present procedure appears particularly in agreement with those obtained with the strategies proposed in [60] and [63], as well as with the experimental results in terms of max base shear and stiffness of the linear path of the curves.

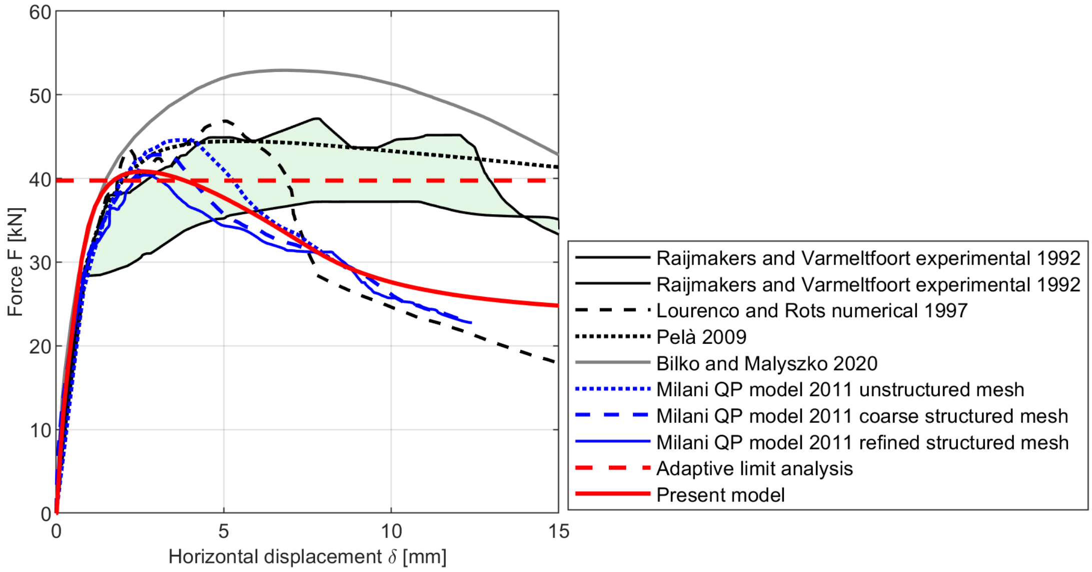

Fig. 11 – Comparison of the present procedure results with other numerical and experimental results.

4 Full-scale case study

The application of the two-step procedure to a full-scale two-storey masonry building is here presented. As shown in Fig. 12, the horizontal projection of the construction is completely described by the 4 perimeter walls, each one 0.25 m thick, which define a rectangle 6.00×4.40 m^2. The overall height is equal to 6.44 m. Some openings are present on the two longitudinal walls, here named as wall A and wall B. The masonry is composed of rectangular bricks and lime mortar. Both storeys are characterized by rigid horizontal floors, sustained by walls A and B and connected to the perimeter walls by concrete edgings. The vertical load given by the floors is equal to 10 kN/m^2. This benchmark comes from the experience within the Italian ReLUIS project [68].

The case study is here analyzed under a horizontal load applied along the longitudinal direction. Considering the different disposition of openings between walls A and B, a non-symmetrical behavior is expected. Two horizontal load cases, LCA and LCB in Fig. 12, have been investigated. In both cases, the horizontal load is proportional to the applied vertical weights, which are the masonry self-weight and the load given by the floors. However, whereas in LCA the horizontal loads are concentrated at floor levels, in LCB each modeled element and each non-structural mass considered is subjected to a horizontal load proportional to its weight.

A NURBS model of this full-scale case study has been realized. Two NURBS surfaces have been used for each wall, one for each storey. An initial mesh composed of quadrangular elements has been used. The initial surfaces representing the longitudinal walls have been subdivided into 4×3 elements, whereas 1×3 elements have been used for transversal walls. Additional surfaces have been used to represent concrete edgings, even if no cracks are supposed to occur within these elements. Analogously to the first numerical examples, the mesh adaptation is performed by moving the nodes that constitute elements' vertices, resulting in a total of 82 parameters.

Limit analyses have been performed by assuming 0.04 MPa as tensile strength, 6.2 MPa as compression strength, cohesion of 0.163 MPa and a tangent of the friction angle of 0.58 in shear. Moreover, a specific weight of 17.5 kN/m^3 has been assigned to masonry. With the aim of providing a more realistic representation of the masonry behavior in shear, a non-associative flow rule has been used in this example.

For both the load cases, a population of 80 individuals and a maximum number of 200 generations have been used within the GA. The final results obtained are depicted in Fig. 13. Results are shown in terms of collapse mechanism and collapse base shear, this last one derived from the horizontal load multiplier. It can be noted that the worst damage is observed at the first storey, where both flexural openings and sliding cracks occurred at all the 4 walls. As already pointed out in [68], LCB typically shows higher base shear than LCA, specifically when the mass of the walls is comparable with the mass of the floors.

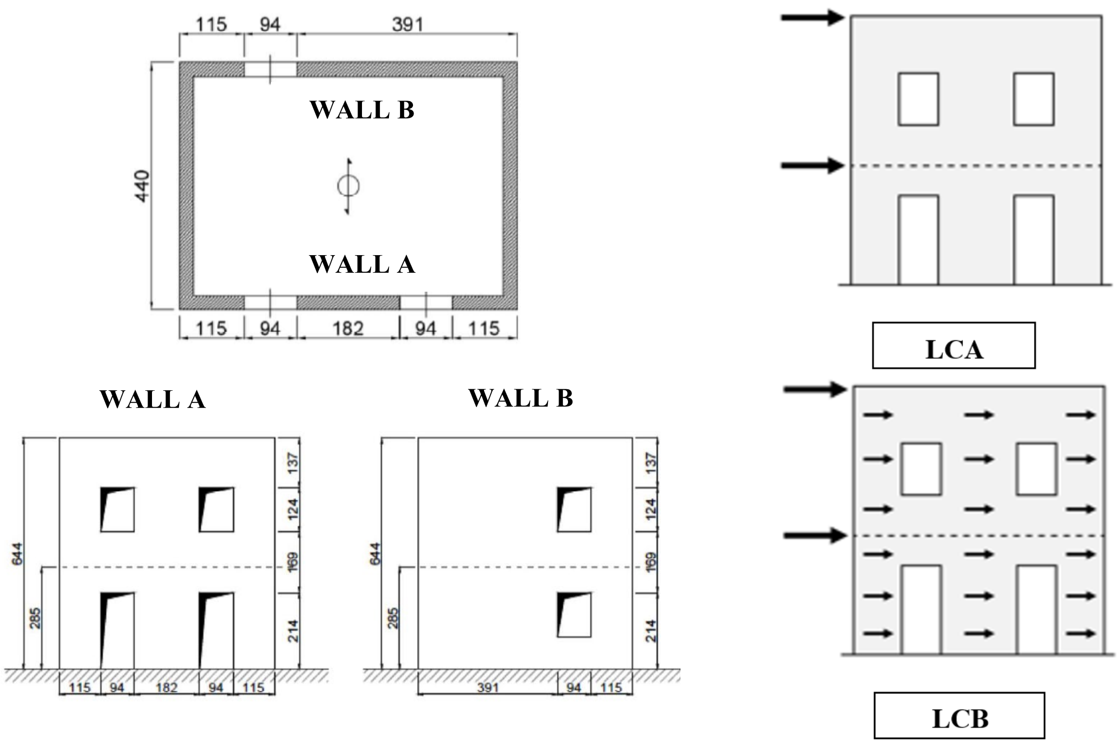

Fig. 12 – Full scale case study: geometry (left, measures in cm) and two load cases considered (right).

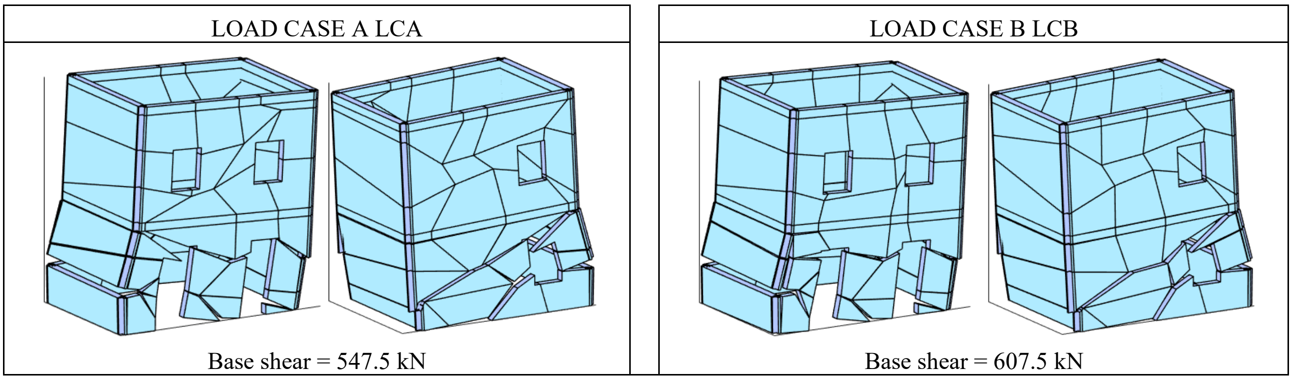

Fig. 13 – Full scale case study: collapse mechanisms and base shear values obtained through adaptive limit analysis.

Concerning the complexity of the collapse mechanism obtained through limit analysis, it appears clear the advantage of introducing the automated import of the geometry, which avoids the time consuming manual modeling of the many different parts that form the actual mechanism.

The model has been studied in Step 2 of the proposed two-step procedure considering the four different hypotheses listed below:

- linear material with constant contact properties, whose mechanical parameters are collected in Table 2;

- linear material with variable contact properties, for which $f_{ty} = f_t$, $G_{fy} = G_f$, $c_y = c$, the ratios between tensile strengths, fracture energies and cohesion in (9) and the relations in (8) have been assumed;
- variable contact properties as above and material with finite compressive strength ("crushing" model in the following), whose CDP properties are collected in Appendix B;
- continuum approach introduced for comparison (see Appendix B for CPD parameters and their calibration).

Table 2. Full scale model parameters.

Material density	w	$[kg/m^3]$	1784
Material Young's modulus	E	$[MPa]$	1800
Material Poisson's coefficient	υ	$[-]$	0.2
Contact cohesion	c	$[MPa]$	0.163
Contact tensile strength	f_t	$[MPa]$	0.04
Contact normal cohesive stiffness	K_{nn}	$[N/m^3]$	5×10^8
Contact shear cohesive stiffness	K_{ss}	$[N/m^3]$	5×10^9
Contact fracture energy	G_f	$[N/m]$	500

The results of the present modelling procedure on a full-scale structure show a good agreement with the base shear values obtained with limit analysis and with those obtained through a continuum approach, in terms of both pushover curves (Fig. 14) and damage pattern (Fig. 15). Indeed, although a comparison between damaged zones appears not trivial due to the differences of the two numerical approaches, it can be observed in Fig. 15 that tensile damage in the continuum models is mainly concentrated at the ground floor as in the present model. Furthermore, the magnitude of compressive damage remains limited for both approaches. Concerning the post-peak response, the continuum model exhibits a plateau, while a considerable softening is shown by the variants of the proposed approach, which is further accentuate in the case with crushing. Accordingly, the proposed approach appears significantly robust and able to account for softening behaviors without numerical issues.

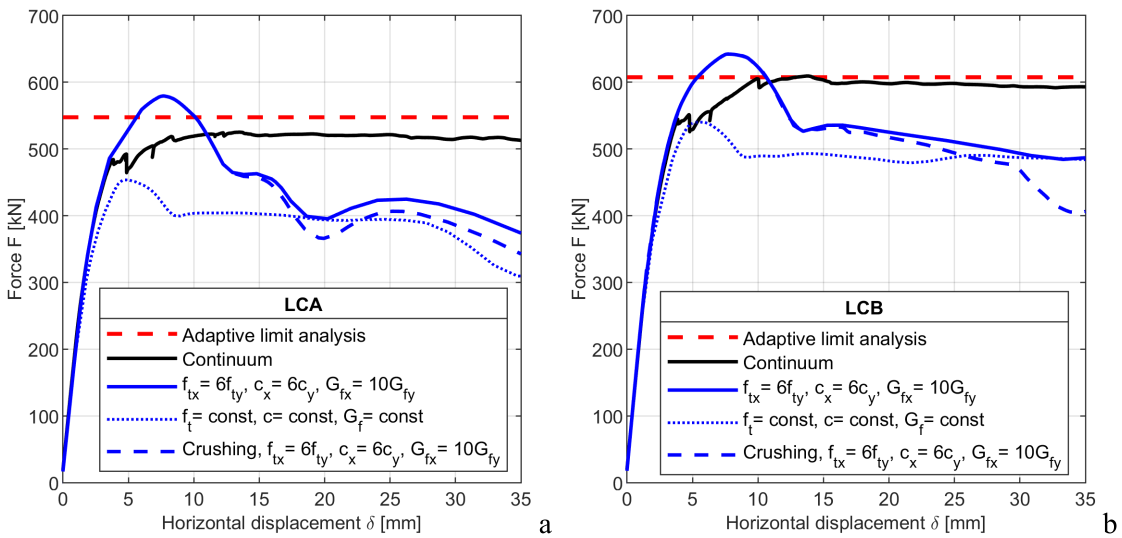

Fig. 14 – Full scale case study analyses results: (a) LCA, (b) LCB.

Furthermore, referring to the time required to run the analyses, the present procedure allows to significantly reduce the computational cost when compared to a standard continuum approach, see Table 3. Being continuum models often the only pursuable strategy when dealing with structures of complex geometry, the proposed procedure herein developed can be surely seen as a performing and efficient alternative to continuum models.

Table 3. Times required to complete the full-scale case study numerical analyses.

	Present model (hh:mm:ss)	Present model ”Crushing” (hh:mm:ss)	Continuum model (hh:mm:ss)
LCA	00:01:54	00:07:51	02:07:24
LCB	00:01:43	00:11:06	02:49:34

Analyses performed on a commercial laptop equipped with a processor Intel Core i7-2670QM 2.20 GHz and 8 GB RAM.

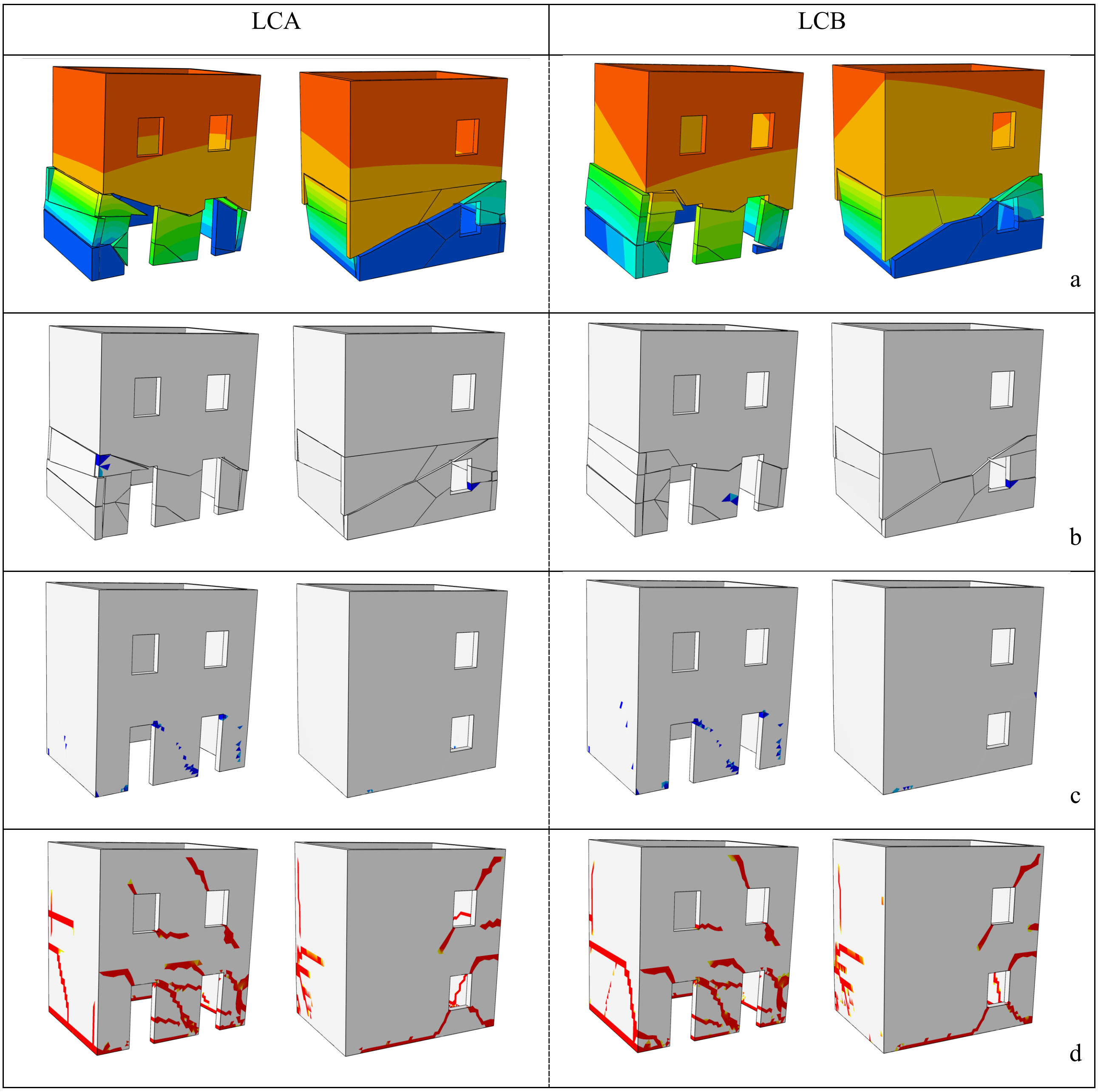

Fig. 15 – Full-scale case study: (a) deformed shapes for the case $f_t = cost$, $G_f = cost$, (b) compressive damage patterns for the case "crushing", (c) compressive and (d) tensile damage patterns for the continuum case.

5 Conclusions

In this paper, a two-step automated procedure based on adaptive limit and pushover analyses has been developed for the seismic assessment of masonry structures. This procedure, originally proposed for the force-displacement description of out-of-plane loaded masonry structures, has been extended to in-plane and combined in- and out-of-plane loading conditions, accounting also for the effect of masonry crushing failure. Accordingly, the generalization of the two-step procedure to in-plane, out-of-plane, and both combined failure modes, accounting also for crushing failures which may appear substantial in many practical cases, appeared particularly appealing for the seismic assessment of historic and ordinary buildings, as it allows to run Standards-based pushover analyses in an efficient and reliable way.

A novel ad-hoc routine has been developed and utilized for the automatic import of the collapse mechanism geometry of any complexity into a solid model ready to be used in a finite element framework. The development of this tool led to an overall enhancement of the procedure efficiency, which is evident from the higher quality that can be reached for the geometry and the reduced amount of time needed for its modelling, particularly when dealing with complex structures.

Mesh refinement appeared to have a minor influence on the structural response. Although a coarse mesh could be adopted without substantially altering the solution, an optimized mesh characterized by a refinement near the contact surfaces has been found to be the best compromise between accuracy and computational effort. Crushing failure has been included in the proposed procedure by means of a nonlinear constitutive law for the portions of the collapse mechanism. Fracture energy of contact-based interfaces was found to significantly influence the pushover curves. Its influence has been investigated through parametric analyses on a windowed shear panel, first considering constant properties for the whole set of interfaces, and then varying them according to relations that account for the orthotropy of masonry.

The proposed procedure has been finally applied to a full-scale case study, where both in-plane and out-of-plane loaded structural elements were present. The results of the proposed procedure in terms of maximum base shear have been found in agreement with the ones obtained through adaptive limit analysis and standard continuum nonlinear analysis for two different load cases. The proposed procedure appeared computationally efficient, particularly if compared to standard continuum models.

Accordingly, the proposed two-step procedure can be considered as a general and efficient method for the reliable seismic assessment of historic and ordinary masonry structures of any geometrical complexity.

ACKNOWLEDGEMENTS

The Authors wish to thank all the partners of the Italian ReLUIS Project - WP10 "Code contributions relating to existing masonry structures" for the fruitful discussions about the full-scale case study.

Appendix A

Here, further details about the Routine 1-to-2 described in Section 2.2 are presented. Particularly, given the collapse mechanism in the form of a figure file, the nodes coordinates of the n patches of the mechanism are retrieved and stored in a structure array A, whose form is:

$$A = \begin{bmatrix} \boldsymbol{x}_1 & \boldsymbol{y}_1 & \boldsymbol{z}_1 \\ \vdots & \vdots & \vdots \\ \boldsymbol{x}_i & \boldsymbol{y}_i & \boldsymbol{z}_i \\ \vdots & \vdots & \vdots \\ \boldsymbol{x}_n & \boldsymbol{y}_n & \boldsymbol{z}_n \end{bmatrix} \qquad (10)$$

where the $\boldsymbol{x}_i$ field is defined as follows:

$$\boldsymbol{x}_i = \left[x_{i1}, \dots, x_{ij}, \dots, x_{im}\right] \qquad (11)$$

being m the number of nodes of the i-th patch. Considering the i-th patch, it is easy to state that its geometry is definitely described once the position of its nodes is known. However, many superfluous nodes lie on the segments between the essential ones, which if not filtered and directly imported in the CAD environment can lead to graphic lags (particularly when dealing with large models) and overabundant nodes that can bring the user to make mistakes more likely. Therefore, a filtering process has been developed to solve this inconvenience. First, keeping unchanged the global reference system used in the figure file, the projections of the i-th patch in the xy, xz and yz planes are derived. Then an algorithm, beginning from the first node, goes forward on the perimeter of each projection of the patch checking the slope of two consecutive segments, described respectively by the node pairs ($j-1$, j) and (j, $j+1$). Established a tolerance $toll_1$ that takes into account imprecisions due to numerical approximation, the algorithm checks the conditions:

$$\begin{aligned} &\left|\frac{x_j - x_{j-1}}{y_j - y_{j-1}} - \frac{x_{j+1} - x_j}{y_{j+1} - y_j}\right| < toll_1 \\ &\left|\frac{x_j - x_{j-1}}{z_j - z_{j-1}} - \frac{x_{j+1} - x_j}{z_{j+1} - z_j}\right| < toll_1 \\ &\left|\frac{z_j - z_{j-1}}{y_j - y_{j-1}} - \frac{z_{j+1} - z_j}{y_{j+1} - y_j}\right| < toll_1 \end{aligned} \qquad (12)$$

If at least one of the conditions in (12) is satisfied, the two checked segments belong to the same straight line, the nodes are therefore discarded and the loop in which the conditions are implemented jumps to the next two segments, described by the nodes pairs (j, $j+1$) and ($j+1$, $j+2$) and so on. In the opposite case, the two segments belong to two different straight lines, the middle node is essential for describing the patch geometry and therefore it is stored to be eventually utilized for the generation of the three-dimensional model in the CAD environment. The process is naturally repeated for all the patches in the structure array. To further strengthen the filtering capacity, another control has been introduced to act when the previous lacks in efficiency, i.e. when nodes laying on segments parallel to the coordinate axes are checked. Once established a new tolerance $toll_2$, the following three conditions are inspected:

$$\begin{aligned} &\left|x_{j+1} - x_{j-1}\right| < toll_2 \quad \& \quad \left|y_{j+1} - y_{j-1}\right| < toll_2 \quad \& \quad z_j \neq z_{j-1} \\ &\left|x_{j+1} - x_{j-1}\right| < toll_2 \quad \& \quad \left|z_{j+1} - z_{j-1}\right| < toll_2 \quad \& \quad y_j \neq y_{j-1} \\ &\left|z_{j+1} - z_{j-1}\right| < toll_2 \quad \& \quad \left|y_{j+1} - y_{j-1}\right| < toll_2 \quad \& \quad x_j \neq x_{j-1} \end{aligned} \qquad (13)$$

If one of the conditions in (13) is satisfied, the checked nodes are on the same segment and thus are discarded, and the algorithm goes forward similarly to what exposed regarding the first filtering approach.

Appendix B

This appendix briefly recalls the CDP model originally developed by Lee and Fenves [69]. It assumes two scalar damage variables d_t and d_c, whose values can vary between zero and one. Under uniaxial tension and compression, the stress-strain relations are:

$$\sigma_t = (1 - d_t)E_0\left(\varepsilon_t - \varepsilon_t^p\right), \quad \sigma_c = (1 - d_c)E_0\left(\varepsilon_c - \varepsilon_c^p\right) \qquad (14)$$

where σ_t and σ_c are the uniaxial stresses in tension and compression, E_0 is the undamaged Young's modulus of the material, ε_t and ε_c are the uniaxial tensile and compressive strains, ε_t^p and ε_c^p are respectively the uniaxial plastic strains in traction and compression.

The model assumes a non-associated potential plastic flow [69], with a plastic potential defined by the dilatancy angle ψ and an eccentricity ϵ acting as a smoothing parameter. The evolution of the yield surface is governed by two hardening variables and depends on a shape constant ρ and on the initial ratio f_{b0}/f_{c0} between the biaxial compressive yield stress f_{b0} and the uniaxial compressive yield stress f_{c0}. The values of the above parameters have been assumed in agreement with the literature for masonry materials [69] [70], see Table 4. The CDP model is then fully characterized by uniaxial stress-strain relationships in tension and compression.

Table 4. CDP model parameters.

ϵ	ψ	f_{b0}/f_{c0}	ρ
0.1	10°	1.16	2/3

In Step 2 of the proposed procedure, material nonlinearities are introduced to account for the possibility of compressive failure. It has to be pointed out that although the CDP model is introduced in this case to account only for damage in compression, it still requires the tensile behaviour to be specified. Accordingly, a tensile strength higher than the strength of the interfaces f_t is assumed.

In Section 4, the CDP model is also used in a full continuum fashion, i.e. standard approach, for comparison. Accordingly, a calibration akin to the one proposed in [71] has been carried out to evaluate the mechanical parameters for the full-scale case study in a standard continuum model framework.

The complete set of CDP parameters used to introduce the crushing damage for the models in Sections 3.2 and 4 and for the standard continuum models in Section 4 are shown in Table 5.

Table 5. CDP uniaxial stress-strain relationships in tension and compression.

Compressive yield stress $[MPa]$		Inelastic strain	Compressive damage variable d_c	Tensile yield stress $[MPa]$		Cracking strain	Tensile damage variable d_t
Crushing implementation							
Models in Sect. 3.2	Models in Sect. 4			Models in Sect. 3.2	Models in Sect. 4		
10.5 (2.5)	6.2	0	0	2	1	0	0
10.5 (2.5)	6.2	0.003	0	0.2	0.1	0.001	0
1.05 (0.25)	0.62	0.01	0.9				
Continuum models in Sect. 4							
5.5		0	0	0.198		0	0
6.2		0.002	0	0.02		0.001	0.9
0.7		0.01	0.9				

REFERENCES

[1] A. M. D'Altri, V. Sarhosis, G. Milani, J. Rots, S. Cattari, S. Lagomarsino, E. Sacco, A. Tralli, G. Castellazzi and S. de Miranda, “Modeling strategies for the computational analysis of unreinforced masonry structures: review and classification,” *Archives of Computational Methods in Engineering,* vol. 27, pp. 1153-1185, 2020.

[2] M. Malena, F. Portioli, R. Gagliardo, G. Tomaselli, L. Cascini and G. de Felice, “Collapse mechanism analysis of historic masonry structures subjected to lateral loads: A comparison between continuous and discrete models,” *Computers & Structures,* vol. 220, pp. 14-31, 2019.

[3] J. Heyman, “The stone skeleton,” *International Journal of Solids and Structures,* vol. 2, no. 2, p. 249–279, 1966.

[4] M. Angelillo, “Static analysis of a Guastavino helical stair as a layered masonry shell,” *Composite Structures,* vol. 119, p. 298–304, 2015.

[5] F. Marmo and L. Rosati, “Reformulation and extension of the thrust network analysis,” *Computers & Structures,* vol. 182, p. 104–118, 2017.

[6] P. Block and J. Ochsendorf, “Thrust network analysis: A new methodology for three-dimensional equilibrium,” *Journal of the International Association for shell and spatial structures,* vol. 48, no. 3, pp. 167-173, 2007.

[7] F. Fraternali, “A thrust network approach to the equilibrium problem of unreinforced masonry vaults via polyhedral stress functions,” *Mechanics Research Communications,* vol. 37, no. 2, p. 198–204, 2010.

[8] A. Iannuzzo, A. Dell'Endice, T. Van Mele and P. Block, “Numerical limit analysis-based modelling of masonry structures subjected to large displacements,” *Computers & Structures,* vol. 242, p. 106372, 2021.

[9] F. Portioli, C. Casapulla, M. Gilbert and L. Cascini, “Limit analysis of 3D masonry block structures with non-associative frictional joints using cone programming,” *Computers & Structures,* vol. 143, p. 108–121, 2014.

[10] C. Baggio and P. Trovalusci, “Limit analysis for no-tension and frictional three-dimensional discrete systems,” *Journal of Structural Mechanics,* vol. 26, no. 3, pp. 287-304, 1998.

[11] L. Cascini, R. Gagliardo and F. Portioli, “LiABlock_3D: A software tool for collapse mechanism analysis of historic masonry structures,” *International Journal of Architectural Heritage,* 2018 doi:10.1080/15583058.2018.1509155.

[12] M. Rossi, C. Calderini, B. Di Napoli, L. Cascini and F. Portioli, “Structural analysis of masonry vaulted staircases through rigid block limit analysis,” *Structures,* vol. 23, pp. 180-190, 2020.

[13] G. Milani, “3D Upper Bound Limit Analysis of Multi-Leaf Masonry Walls,” *International Journal of Mechanical Sciences,* vol. 50, no. 4, p. 817–836, 2008.

[14] G. Milani and P. Lourenço, “A simplified homogenized limit analysis model for randomly assembled blocks out-of-plane loaded,” *Computers & Structures,* vol. 88, p. 690–717, 2010.

[15] A. Cavicchi and L. Gambarotta, “Two-dimensional finite element upper bound limit analysis of masonry bridges,” *Computers & structures,* vol. 84, no. 31-32, pp. 2316-2328, 2006.

[16] S. Sloan and P. Kleeman, “Upper Bound Limit Analysis Using Discontinuous Velocity Fields,” *Computer Methods in Applied Mechanics and Engineering,* vol. 127, no. 1-4, p. 293–314, 1995 doi:10.1016/0045-7825(95)00868-1.

[17] G. Milani, “ Upper bound sequential linear programming mesh adaptation scheme for collapse analysis of masonry vaults,” *Advances in Engineering Software,* vol. 79, p. 91–110, 2015.

[18] A. Chiozzi, G. Milani and A. Tralli, “A Genetic Algorithm NURBS-based new approach for fast kinematic limit analysis of masonry vaults,” *Computers & Structures,* vol. 182, p. 187–204, 2017.

[19] A. Chiozzi, G. Milani, N. Grillanda and A. Tralli, “A fast and general upper-bound limit analysis approach for out-of-plane loaded masonry walls,” *Meccanica,* vol. 53, no. 7, pp. 1875-1898, 2018.

[20] M. Godio and K. Beyer, “Evaluation of force-based and displacement-based out-of-plane seismic assessment methods for unreinforced masonry walls through refined model simulations,” *Earthquake Engineering & Structural Dynamics,* vol. 48, no. 4, p. 454–475, 2018.

[21] C. Chácara, F. Cannizzaro, B. Pantò, I. Caliò and P. B. Lourenço, “Seismic vulnerability of URM structures based on a Discrete Macro-Element Modeling (DMEM) approach,” *Engineering Structures,* vol. 201, p. 109715, 2019.

[22] S. Lagomarsino, A. Penna, A. Galasco and S. Cattari, “TREMURI program: An equivalent frame model for the nonlinear seismic analysis of masonry buildings,” *Engineering Structures,* vol. 56, p. 1787–1799, 2013.

[23] N. Chieffo, F. Clementi, A. Formisano and S. Lenci, “Comparative fragility methods for seismic assessment of masonry buildings located in Muccia (Italy),” *Journal of Building Engineering,* vol. 25, p. art. no. 100813 , 2019.

[24] G. Chiumiento and A. Formisano, “Simplified and refined analyses for seismic investigation of historical masonry clusters: Comparison of results and influence of the structural units position,” *Frontiers in Built Environment,* vol. 5, p. art. no. 84, 2019.

[25] A. Formisano and A. Massimilla, “A Novel Procedure for Simplified Nonlinear Numerical Modeling of Structural Units in Masonry Aggregates,” *International Journal of Architectural Heritage,* vol. 12, no. 7-8, pp. 1162-1170, 2018.

[26] A. Formisano and A. Marzo, "Simplified and refined methods for seismic vulnerability assessment and retrofitting of an Italian cultural heritage masonry building," *Computers and Structures,* vol. 180, pp. 13-26, 2017.

[27] D. Malomo and M. J. DeJong, "A Macro-Distinct Element Model (M-DEM) for simulating the in-plane cyclic behavior of URM structures," *Engineering Structures,* vol. 227, p. 111428, 2021.

[28] D. Baraldi and A. Cecchi, "Discrete Approaches for the Nonlinear Analysis of in Plane Loaded Masonry Walls: Molecular Dynamic and Static Algorithm Solutions," *European Journal of Mechanics - A/Solids,* vol. 57, p. 165–177, 2016.

[29] A. M. D'Altri, F. Messali, J. Rots, G. Castellazzi and S. de Miranda, "A damaging block-based model for the analysis of the cyclic behaviour of full-scale masonry structures," *Engineering Fracture Mechanics,* vol. 209, pp. 423-448, 2019.

[30] R. Serpieri, M. Albarella and E. Sacco, "A 3D Microstructured Cohesive–frictional Interface Model and Its Rational Calibration for the Analysis of Masonry Panels," *International Journal of Solids and Structures,* vol. 122–123, p. 110–127, 2017.

[31] L. Cascini, F. Portioli and R. Landolfo, "3D Rigid block micro-modelling of a full-scale unreinforced brick masonry building using mathematical programming," *International Journal of Masonry Research and Innovation,* vol. 1, no. 3, pp. 189-206, 2016.

[32] M. Angelillo, A. Fortunato, A. Gesualdo, A. Iannuzzo and G. Zuccaro, "Rigid block models for masonry structures," *International Journal of Masonry Research and Innovation,* vol. 3, no. 4, pp. 349-368, 2018.

[33] D. Addessi and E. Sacco, "Nonlinear analysis of masonry panels using a kinematic enriched plane state formulation," *International Journal of Solids and Structures,* vol. 90, pp. 194-214, 2016.

[34] M. Petracca, L. Pelà, R. Rossi, S. Oller, G. Camata and E. Spacone, "Regularization of first order computational homogenization for multiscale analysis of masonry structures," *Computational Mechanics,* vol. 57, no. 2, pp. 257-276, 2015.

[35] M. Valente, G. Milani, E. Grande and A. Formisano, "Historical masonry building aggregates: advanced numerical insight for an effective seismic assessment on two row housing compounds," *Engineering Structures,* vol. 190, pp. 360-379, 2019.

[36] L. Pelà, *Continuum damage model for nonlinear analysis of masonry structures, PhD thesis.,* Universitat Politècnica de Catalunya, 2009.

[37] M. F. Funari, S. Spadea, P. Lonetti, F. Fabbrocino and R. Luciano, "Visual programming for structural assessment of out-of-plane mechanisms in historic masonry structures," *Journal of Building Engineering,* vol. 31, p. 101425, 2020.

[38] T. Forgács, V. Sarhosis and K. Bagi, "Influence of construction method on the load bearing capacity of skew masonry arches," *Engineering Structures,* vol. 168, no. 1, pp. 612-627 , 2018.

[39] A. Ferrante, F. Clementi and G. Milani, “Advanced numerical analyses by the Non-Smooth Contact Dynamics method of an ancient masonry bell tower,” *Mathematical Methods in the Applied Sciences,* vol. 43, no. 13, pp. 7706-7725, 2020.

[40] J. Lemos, “Contact representation in rigid block models of masonry,” *International Journal of Masonry Research and Innovation,* vol. 4, no. 321-334, p. 2, 2017.

[41] F. Clementi, A. Ferrante, E. Giordano, F. Dubois and S. Lenci, “Damage assessment of ancient masonry churches stroked by the Central Italy earthquakes of 2016 by the non-smooth contact dynamics method,” *Bulletin of Earthquake Engineering,* vol. 18, no. 2, pp. 455-486, 2020.

[42] V. Sarhosis and J. Lemos, "A detailed micro-modelling approach for the structural analysis of masonry assemblages," *Computers and Structures,* vol. 206, no. 1, pp. 66-81, 2018.

[43] V. Sarhosis, S. Garrity and Y. Sheng, “Influence of brick-mortar interface on the mechanical behaviour of low bond strength masonry brickwork lintels,” *Engineering Structures,* vol. 88, no. 1, pp. 1-11, 2015.

[44] G. Uva, V. Tateo and S. Casolo, “Presentation and validation of a specific RBSM approach for the meso-scale modelling of in-plane masonry-infills in RC frames,” *International Journal of Masonry Research and Innovation,* vol. 5, no. 3, pp. 366-395, 2020.

[45] Ž. Nikolić, H. Smoljanović and N. Živaljić, “Numerical analysis of masonry structures by finite-discrete element model,” *International Journal of Masonry Research and Innovation,* vol. 1, no. 4, pp. 330-350, 2016.

[46] V. Sarhosis, K. Tsavdaridis and I. Giannopoulos, "Discrete element modelling of masonry infilled steel frames with multiple window openings subjected to lateral load variations," *Open Construction and Building Technology Journal,* vol. 8, no. 1, pp. 93-103 , 2014.

[47] V. Gazzani, M. Poiani, F. Clementi, G. Milani and S. Lenci, “Modal parameters identification with environmental tests and advanced numerical analyses for masonry bell towers: a meaningful case study,” *Procedia Structural Integrity,* vol. 11, pp. 306-313, 2018.

[48] A. Ferrante, D. Loverdos, F. Clementi, G. Milani, A. Formisano, S. Lenci and V. Sarhosis, “Discontinuous approaches for nonlinear dynamic analyses of an ancient masonry tower,” *Engineering Structures,* vol. 230, p. 111626, 2021.

[49] F. Clementi, G. Milani, A. Ferrante, M. Valente and S. Lenci, “Crumbling of Amatrice clock tower during 2016 Central Italy seismic sequence: Advanced numerical insights,” *Frattura Ed Integrità Strutturale,* vol. 14, no. 51, p. 313–335, 2019.

[50] M. Pepe, M. Pingaro, P. Trovalusci, E. Reccia and L. Leonetti, "Micromodels for the in-plane failure analysis of masonry walls: Limit analysis, FEM and FEM/DEM approaches," *Frattura e Integrità Strutturale,* vol. 14, no. 51, pp. 504-516, 2020.

[51] D. Baraldi, C. De Carvalho Bello, A. Cecchi, E. Meroi and E. Reccia, "Nonlinear behavior of masonry walls: FE, DE, and FE/DE models," *Composites: Mechanics, Computations, Applications,* vol. 10, no. 3, pp. 253-272 , 2019.

[52] D. Baraldi, E. Reccia and A. Cecchi, "In plane loaded masonry walls: DEM and FEM/DEM models. A critical review," *Meccanica,* vol. 53, no. 7, pp. 1613-1628, 2018.

[53] A. M. D'Altri, S. de Miranda, G. Milani and G. Castellazzi, "A numerical procedure for the force-displacement description of out-of-plane collapse mechanisms in masonry structures," *Computers & Structures,* vol. 233, no. 106234, 2020.

[54] P. Fajfar, "Fajfar, P. (2000). A nonlinear analysis method for performance-based seismic design," *Earthquake spectra,* vol. 16, no. 3, pp. 573-592, 2000.

[55] L. Piegl and W. Tiller, The NURBS Book, Springer, 1995.

[56] N. Grillanda, A. Chiozzi, G. Milani and A. Tralli, "Efficient meta-heuristic mesh adaptation strategies for NURBS upper–bound limit analysis of curved three-dimensional masonry structures," *Computers & Structures,* vol. 236, p. 106271, 2020.

[57] R. L. Haupt and S. E. Haupt, Practical genetic algorithms, John Wiley & Sons, 2004.

[58] N. Grillanda, A. Chiozzi, G. Milani and A. Tralli, "Collapse behavior of masonry domes under seismic loads: an adaptive NURBS kinematic limit analysis approach," *Engineering Structures,* vol. 200, p. 109517, 2020.

[59] N. Grillanda, A. Chiozzi, G. Milani and A. Tralli, "Tilting plane tests for the ultimate shear capacity evaluation of perforated dry joint masonry panels. Part II: Numerical analyses Engineering Structures," *Engineering Structures,* 2020 (in press).

[60] P. Lourenço and J. Rots, "A multi-surface interface model for the analysis of masonry structures.," *Journal of Engineering Mechanics,* vol. 123, no. 7, pp. 660-668, 1997.

[61] *Abaqus®. Theory manual, Version 6.17, 2017.*

[62] T. Raijmakers and A. Vermeltfoort, "Deformation controlled tests in masonry shear walls. Report B-92-1156," Delft, 1992.

[63] G. Milani, "Simple omogenization model for the non-linear analysis of in-plane loaded masonry walls," *Computers & Structures,* vol. 89, pp. 1586-1601, 2011.

[64] G. Milani and E. Bertolesi, "Quasi-analytical homogenization approach for the non-linear analysis of in-plane loaded masonry panels.," *Construction and Building Materials,* vol. 146, no. 15, p. 723–743, 2017.

[65] R. Van der Pluijm, R. Rutten and C. Schiebroek, “Flexural behavior of masonry in different directions,” in *Proceedings of the 4th international masonry conference IMC4*, London, 1992.

[66] P. B. Lourenço, “An anisotropic macro-model for masonry plates and shells: Implementation and validation,” PhD Dissertation, Delft University of Technology, Delft, 1997.

[67] P. Bilko and L. Malyszko, “An orthotropic elastic-plastic constitutive model for masonry walls,” *Materials,* vol. 13, no. 18, p. 4064, 2020.

[68] F. Cannizzaro, B. Pantò, G. Castellazzi, G. Camata, M. Petracca and N. Grillanda, “Modelling the seismic response of a 2-storey URM benchmark case study. Part II: Comparison among different modelling strategies using two and three dimensional elements,” *Submitted to Bulletin of Earthquake Engineering, SI on "URM nonlinear modelling-Benchmark project",* 2020.

[69] J. Lee and G. L. Fenves, “Plastic-Damage Model for Cyclic Loading of Concrete Structures,” *Journal of Engineering Mechanics,* vol. 124, no. 8, p. 892–900, 1998 doi:10.1061/(asce)0733-9399(1998)124:8(892).

[70] G. Milani, M. Valente and C. Alessandri, “The Narthex of the Church of the Nativity in Bethlehem: A Non-Linear Finite Element Approach to Predict the Structural Damage,” *Computers & Structures,* 2017 doi:10.1016/j.compstruc.2017.03.010.

[71] A. M. D'Altri, F. Cannizzaro, M. Petracca and D. Talledo, “Nonlinear modelling of the seismic response of masonry structures: Calibration strategies,” *Submitted to Bulletin of Earthquake Engineering, SI on "URM nonlinear modelling-Benchmark project",* 2020.